Lidar Observations of Airfield Approach Conditions: An Exploratory Study[1]

W. VIEZEE, E. E. UTHE AND R. T. H. COLLIS
Stanford Research Institute, Menlo Park, Calif.

(Manuscript received 9 December 1968, in revised form 9 January 1969)

ABSTRACT

Lidar (laser radar) data obtained at Hamilton AFB, Calif., under conditions of low ceiling and visibility, are analyzed by hand and by electronic computer to explore the operational utility of lidar in determining cloud ceiling and visibility for aircraft landing operations. Hand analyses of the data show the ability of the lidar to describe the spatial configuration of the low-cloud structure in the direction of the landing-approach path. The problems inherent in evaluating lidar observations are discussed, and initial approaches to quantitative solutions by computer are presented. It is demonstrated that operationally useful information on the ceiling conditions contained in the hand analyses can be represented by digitizing the lidar data and subjecting these data to computer analysis.

1. Introduction

In order to explore the operational utility of lidar (laser radar) in aircraft landing operations under conditions of low ceiling and poor visibility, Stanford Research Institute (SRI) operated a pulsed ruby lidar at Hamilton AFB, Calif., in January 1968. Because of a unique location of the airfield on the western edge of San Pablo Bay (Fig. 1), the aircraft landing operations are confronted with a difficult meteorological problem. San Pablo Bay with its relatively cold water is a notorious source of fog and low stratus, particularly in winter. The landing-approach glide path begins over the marshes and open water of the Bay, an area characterized by low ceiling and visibility, and extends 6 mi, with a 2.5° slope, to the point of touchdown. The Air Weather Service observing station and a rotating-beam ceilometer are located near touchdown, i.e., as near as possible to the area of deteriorating ceiling and visibility (Fig. 1). However, even at this forward location, ceiling and visibility conditions are often quite different from those encountered by incoming aircraft over the marshes and open water.

The observations, carried out at the request of local Air Force authorities, were restricted to a two-day period (8–9 January) and are incomplete in many respects (for example, the only lidar available at the time was a ruby system with a limited data-collection rate of 2 pulses min^{-1}). The observations provided an adequate basis, however, for the analyses described below and for an assessment of the way in which lidar can be used with advantage at Hamilton AFB, or indeed at any airfield, for remotely monitoring conditions along the landing approach path.

[1] The research on which this article is based was supported in part by Stanford Research Institute, in part by the Aerospace Instrumentation Laboratory of AFCRL under Contract No. F19628-68-C-0021, and in part by the Naval Air Systems Command.

2. Method of observations and data analysis

The SRI Mark V pulsed ruby lidar, details of which are given in Table 1, was transported to Hamilton AFB and placed next to the weather observing station and the rotating-beam ceilometer. Data related to cloud ceiling and visibility were collected by firing at a pulse rate frequency of 1 or 2 pulses min^{-1} out across the Bay, parallel to the aircraft glide path (Fig. 1). The elevation angle of the direction of firing was varied from 0 to 65° without change of azimuth. All data were obtained under the actual weather conditions that created the operational problems. The weather conditions that prevailed during the period of lidar operation are given in Table 2.

Each lidar firing was separately recorded by photographing the analog trace of received signal power vs

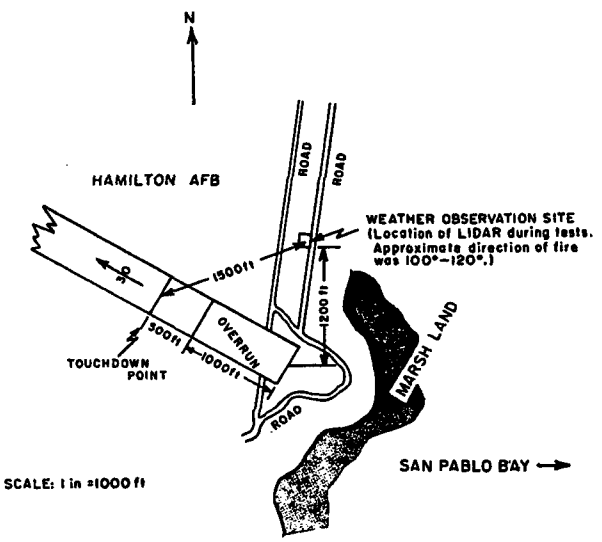

FIG. 1. Location of SRI lidar at Hamilton AFB relative to touchdown point and to San Pablo Bay.

TABLE 1. Characteristics of SRI Mark V ruby lidar.

Transmitter	
Laser	6×⅜ inch ruby crystal, Brewster-angle one end, planar one end, uncoated
Q-switch	Rotating prism and saturable dye
Wavelength	6943 Å
Pulse length	15 nsec
Peak power	18 MW
Pulse energy output	0.27 joule
Optics	6-inch Newtonian reflector telescope
Beamwidth	Approximately 0.3 mrad
PRF	Two per minute
Receiver	
Photomultiplier	14-stage RCA type 7265
Optics	6-inch Newtonian reflector telescope with adjustable field stop
Beamwidth	0.2–0.9 mrad
Bandpass	Approximately 17 Å

TABLE 2. Weather conditions during lidar observations at Hamilton AFB.

Weather conditions	8 January 1968	9 January 1968
Cloud ceiling	700–800 ft	400–500 ft
Prevailing visibility	1½–2½ mi	¼–½ mi
Obstruction to visibility	Fog, occasional light rain	Fog, light drizzle
Temperature	37–38F	39–40F

slant range (often called the backscatter signature) as it appeared on the oscilloscope ("A scope").

Fig. 2 shows examples of lidar data obtained at three elevation angles. The received signal power on a logarithmic scale is recorded vs slant range on a linear scale. The use of a logarithmic video amplifier in the receiver is almost essential in order to compress the wide dynamic range of the detector (typically four or more orders of magnitude) and to enable the received signal to be displayed on a single oscilloscope trace without loss of detailed information. The sweep speed of the oscilloscope in Figs. 2b and 2c is twice as fast (1 μsec per division with a maximum recorded range of 1.5 km) as that in Fig. 2a (2 μsec per division with a maximum recorded range of 3.0 km) in order to show the significant lidar "echoes" detected at the higher elevation angles in more detail. At close-in ranges (up to about 100 m), the receiver output increases rapidly as the diverging transmitted beam of the non-coaxial lidar system gradually merges with the diverging receiver field of view. The point of full beam convergence lies near the peak of the curve, i.e., near the point of maximum signal amplitude at the bottom of the photograph. In Fig. 2a the receiver output reaches a maximum near the point of full beam convergence at a range of 100–120 m, after which it decreases as the range to the fog particles producing the backscatter increases.

If large inhomogeneities such as cloud layers are present along the path, the strength of the return signal may suddenly increase and/or decrease as shown in Figs. 2b and 2c. In the present experiment a rapid increase in received power followed by a decrease is considered as an echo related to a cloud *layer*, while a single rapid decrease (Fig. 2b) is related to a *level* of large change in the transmitted signal attenuation. This large change in attenuation can arise from either a rapid increase or a rapid decrease in the optical density of the fog or clouds. Layers and levels observed by the lidar during one complete "scan" from the horizontal to the near vertical are analyzed and related to the low cloud structure and the cloud ceiling as measured by the ceilometer.

Following SRI's routine safety practices, at any time the lidar was capable of being fired, either intentionally or accidentally, its field of view (which is physically limited to a definite sector) was kept under surveillance. Specifically, when an observation was made the operator monitored the field of view of the coaligned aiming telescope, to ensure that no aircraft were near the aiming point. Whenever the unit was unattended, its capacitance banks were discharged and it was rendered inoperative.

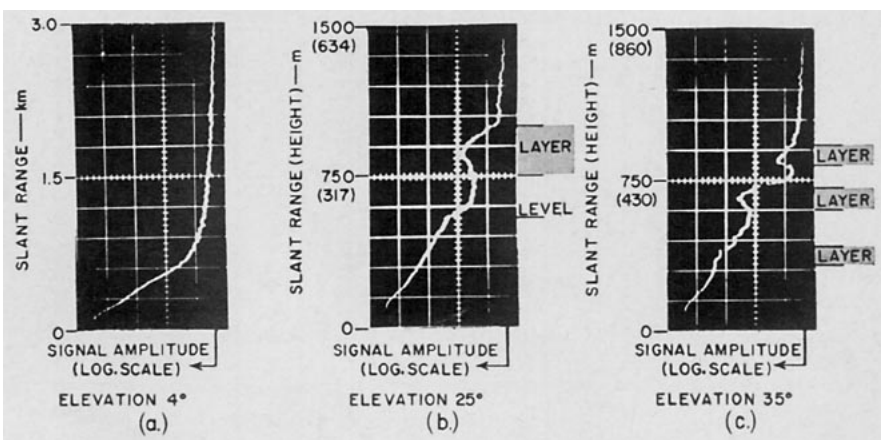

FIG. 2. Samples of lidar data obtained at Hamilton AFB, under conditions of low ceiling and visibility.

These measures are possibly excessively cautious in view of the many factors that limit the hazard to human eyesight—the very narrow beam, the low firing rate, the briefness of the pulse, the attenuation of the atmosphere, the attenuation of the aircraft's cockpit canopy, etc. However, they are considered to be good experimental practice. For any subsequent routine operational application of lidar, due consideration must be given to the question of safety. The unattended use of high peak power lidars, especially those operating in the visible spectrum, is not recommended. Preferable alternatives are to use higher pulse-rate systems of lower peak power, and wavelengths outside the visible spectrum.

3. Lidar observations related to cloud ceiling

a. Hand analysis of available data

Fig. 3 presents the spatial distribution of the low-level cloud layers as observed with the lidar in the direction of San Pablo Bay during three separate time periods on 8 January 1968. The spatial distributions are

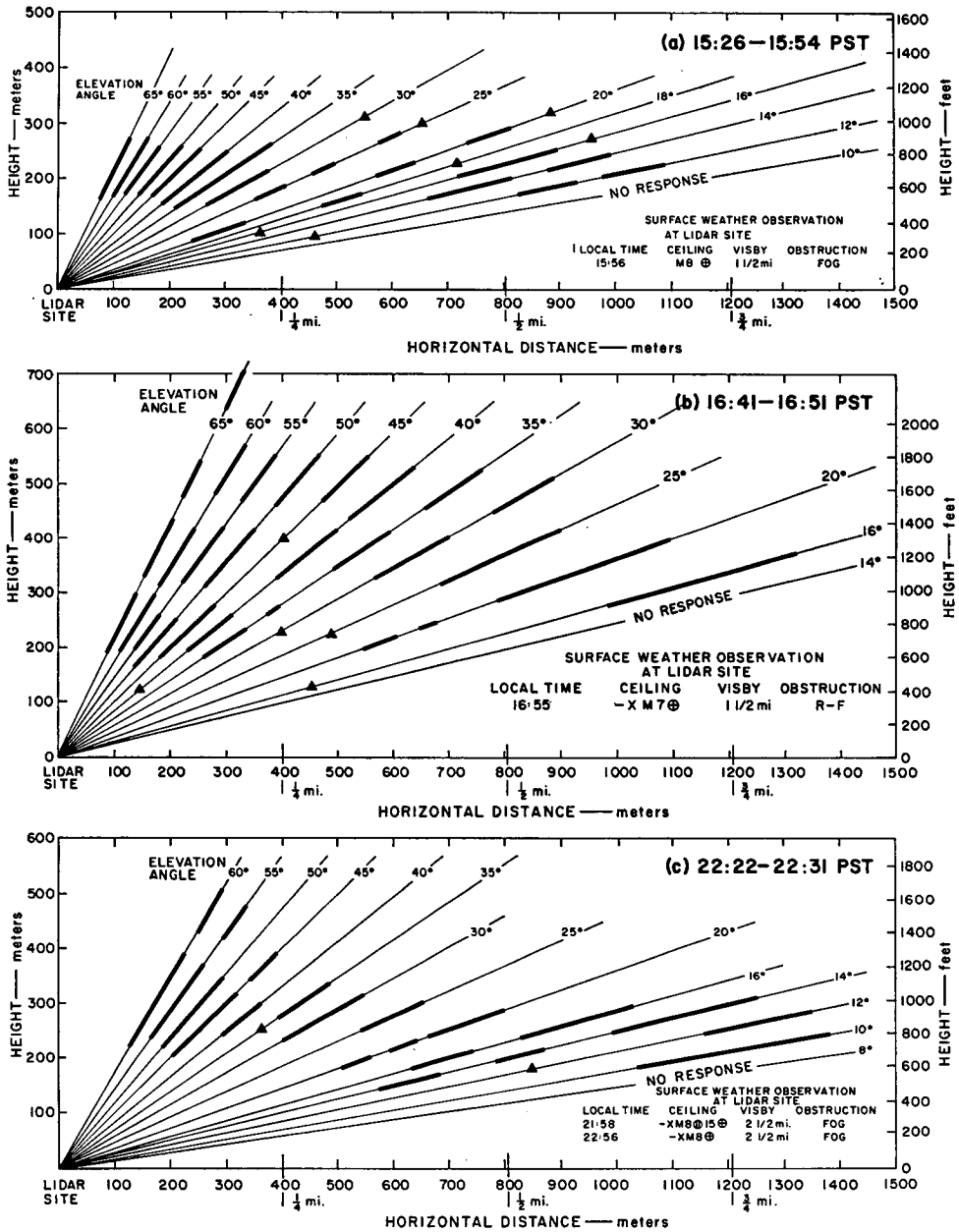

FIG. 3. Spatial distribution of low clouds detected by lidar at Hamilton AFB on 8 January 1968 (solid bars: cloud layers; solid triangles: levels of optical density change).

obtained by firing the lidar at successive elevation angles from a maximum of 65° down to the horizontal, and by identifying, along each direction of firing, all echoes related to cloud layers and to levels of optical density change. Layers are indicated by solid bars and levels by solid triangles. Also indicated in each figure is the available surface-weather observation for the time closest to the period of the lidar data. Observed cloud-ceiling height (in hundreds of feet) is given by the ceilometer. Observed horizontal visibility is the so-called prevailing visibility defined as "the greatest visibility that is attained or surpassed throughout at least half of the horizon circle, not necessarily continuous."

Fig. 3 shows that under the prevailing weather conditions the lidar is capable of describing the low-cloud structure from the observation site out to a distance of 0.8–1.2 km ($\frac{1}{2}$–$\frac{3}{4}$ mi). This relatively limited range is due to the large attenuation of the lidar pulse energy along the slant paths through the fog at low elevation angle. During the evening, when the reported horizontal visibility increased from $1\frac{1}{2}$–$2\frac{1}{2}$ mi, the cloud base could be detected to ranges of $\frac{3}{4}$ mi. The cloud-ceiling height measured at the observation site by the rotating-beam ceilometer corresponded to the height of the lowest layer of lidar echoes obtained at high elevation angle.

Fig. 3a shows a marked difference in the lidar-detected cloud structure between elevation angles larger and less than about 35°. This difference probably arises from the fact that at high elevation angle the low cloud echoes are detected at close range, with a subsequent loss of resolution in the recorded lidar trace. Under such conditions a change in the sweep speed of the "A scope" must be used to "magnify" the lidar trace.

Figs. 3b and 3c show that higher level cloud layers are detected only at the high elevation angles, where the path length through the lower clouds and the fog is minimum. The ceilometer detected higher cloud layers only during the time period of Fig. 3c when the ceiling was broken.

Fig. 4 illustrates the capability of the SRI ruby lidar to remotely monitor cloud-ceiling variations at a point distant from the observation site. It shows a 12-min time section of the low-level cloud structure over the Bay at points approximately $\frac{1}{2}$–$\frac{3}{4}$ mi from the lidar site (14° elevation angle) during the afternoon of 8 January. The time period corresponds to that of Fig. 3a. The levels of signal increase, peak signal return and signal decrease, monitored at time intervals of about 30 sec, are indicated and joined by straight line segments to portray the time variation of a 100-m thick low-cloud layer; practically no change with time is evident. Conditions at the remote locations are nearly identical to those "overhead" at the observation site, the height of the peak signal return being nearly identical to the ceiling height given by the ceilometer.

During the morning of 9 January, very low ceiling and visibility prevailed. Up to 1157 PST the sky cover remained overcast, with the cloud base varying between 400 ft (122 m) and 500 ft (152 m). The prevailing horizontal visibility remained around $\frac{1}{2}$ mi (0.8 km) in light drizzle and fog (see Table 1). At 1157, the clouds became broken. Fig. 5 illustrates some typical lidar backscatter profiles obtained throughout the morning at 30° elevation. The rapid decrease in return signal amplitude observed at a height near 492 ft (150 m) at 1153 must be interpreted as due to a rapid increase in optical density, since this height corresponds to that of the cloud ceiling measured by the ceilometer at the lidar site. Furthermore, at 1150 an airborne weather observer[2] reported a 400-ft (140 m) cloud ceiling at 1 mi from touchdown and indicated that clouds ex-

[2] Capt. R. H. Hedenberg, Commander, Det. 9, 35th Weather SQ., Hamilton AFB.

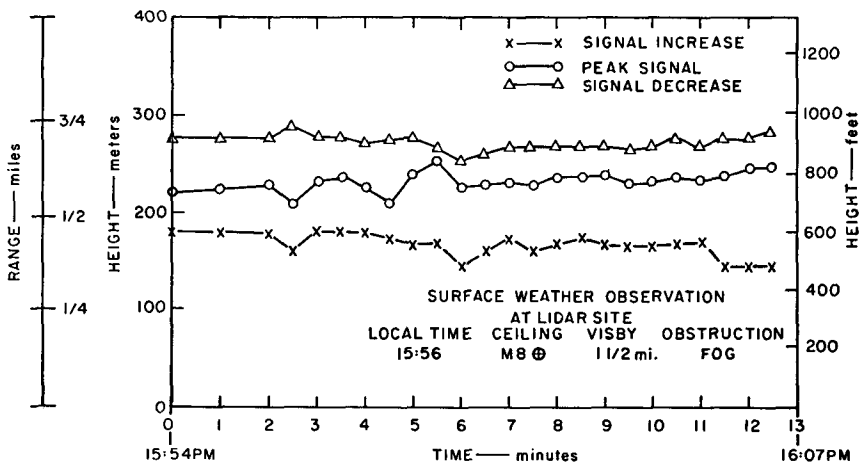

FIG. 4. Time variation of low cloud structure monitored by lidar at $\frac{1}{2}$–$\frac{3}{4}$ mi from the lidar site at Hamilton AFB during afternoon of 8 January 1968.

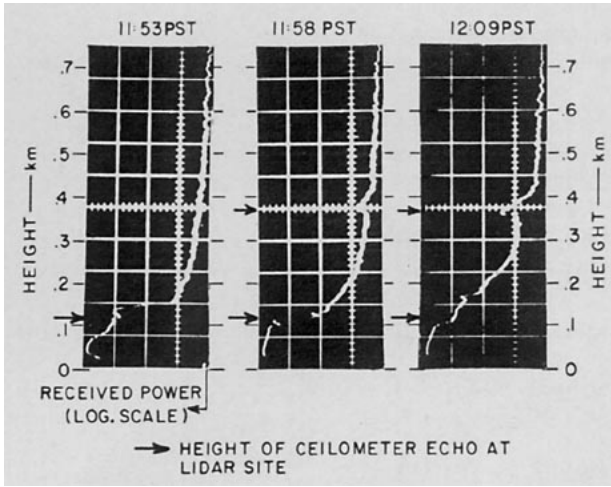

FIG. 5. Samples of lidar data obtained at 30° elevation angle at Hamilton AFB on 9 January 1968.

tended vertically to at least 2000 ft (610 m). Near 1200, however, this dense lower layer became transparent, as evident by the appearance of a cloud echo near 360 m in the lidar profile of 1158 PST. The higher level cloud layer was also detected by the ceilometer at the lidar site and was first reported in the surface weather observation at 1157. Fig. 6 shows the spatial extent of the significant layers and levels detected by the lidar shortly after noon. The lowest-altitude signals correspond to the 400-ft broken-cloud layer indicated by the ceilometer. Agreement between ceilometer and lidar data extends to 1200 ft.

b. Discussion

The data samples analyzed in Figs. 3–6 demonstrate the advantages and limitations of the lidar in the description of the low-level cloud structure under adverse weather conditions. The pulsed lidar can provide a vertical density profile through low-level clouds and, furthermore, because of its ability to operate under variable elevation and azimuth, can accurately describe the spatial distribution of the cloud ceiling. A most useful feature of the lidar is its ability to monitor the cloud-ceiling conditions at a location that is remotely situated with respect to the lidar site. Under the weather conditions that prevailed during the Hamilton AFB experiment, the lidar could accurately monitor the cloud ceiling at a point $\frac{1}{2}$–$\frac{3}{4}$ mi from touchdown point. On the other hand, it was disappointing that the maximum range at which the low clouds could be accurately described remained well below the distance at which the landing approach path intersected the cloud base (1–3 mi). During the fog and light rain or drizzle conditions that prevailed during the experiment, the ruby lidar pulse energy rapidly attenuated down to the noise level over the long slant paths at elevation angles <10–$15°$. Improvement in the range of cloud-mapping capability can be expected in the future by further narrowing the transmitted lidar beam and by introducing higher power output. Such improvements may enable the lidar to obtain an extended range profile of the cloud conditions at an elevation angle equal to that of the landing approach glide path. The lidar data also show a high spatial correlation with the spot information provided by the ceilometer. Under the fog and drizzle conditions that prevailed during the experiment, the ceilometer reading appeared equally valid for locations up to $\frac{1}{2}$–$\frac{3}{4}$ mi away.

4. Computer techniques for analyzing lidar data related to cloud ceiling

a. Computer Analysis of Data Sample

In order to digitize the recorded lidar data for input into a computer program, Polaroid prints of the oscilloscope-displayed lidar signatures, such as shown in Fig. 2, are projected onto the screen of a scaling machine (digitizer) that records on IBM cards the X, Y co-

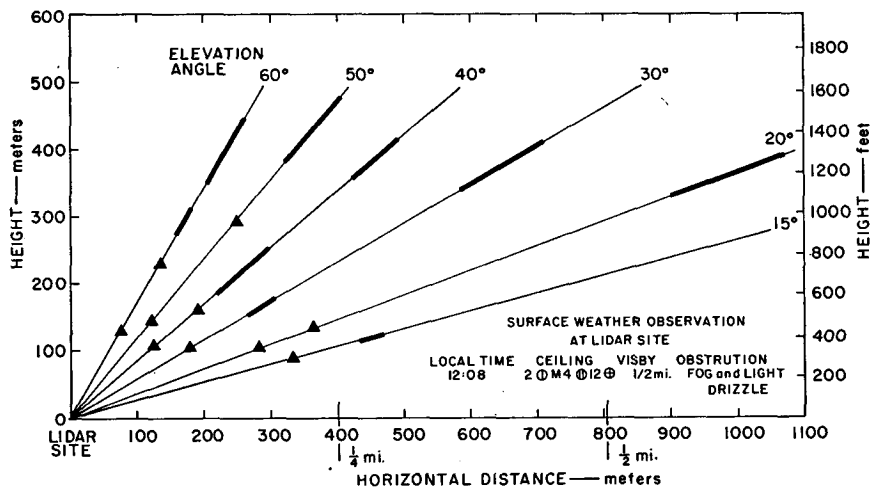

FIG. 6. Same as Fig. 3 except for 9 January 1968, 1207–1211 PST.

ordinates of a movable crosshair. The operator records X, Y values of all inflection points on a lidar recorded signature that, when joined by straight lines, provide a digitized representation of the signature. The X, Y representation of each lidar signature thus obtained constitutes the input for a computer program, which, by use of the digitizer calibration and the beam elevation angle, converts the X, Y values into a matrix of oscilloscope deflection (output voltage) of the data points and a matrix of position of the data points. Such output data from multiple laser firings obtained as the lidar scans from the horizontal to the near vertical are then fed into a grid-point-analysis program formulated by Mr. R. L. Mancuso of SRI (Endlich and Mancuso, 1968). This program assigns a value of the dependent variable (in this case, oscilloscope deflection in volts) to each grid point of a predetermined grid in the vertical plane of observation. Values to individual grid points are assigned on the basis of the five data points nearest to the grid point with the aid of a distance-weighting factor as well as a vector weight defined in the radial direction (which gives more weight to data from a single lidar profile) or in the horizontal direction (which gives added weight to existing conditions of horizontal stratification).

Fig. 7a shows the results of this type of computer analysis using the lidar data observed during the evening of 8 January 1968 (2222–2231 PST). The analysis is prepared from the data of 18 individual lidar profiles obtained at elevation angles ranging from 0 to 60°. In Fig. 7a and in all subsequent figures, coordinate axes and isopleths are drawn by hand. In order to supply as much input data as possible to the grid-point-analysis program, data points intermediate to the inflections were obtained by linear interpolation within the computer program. Minimum distance between lidar-

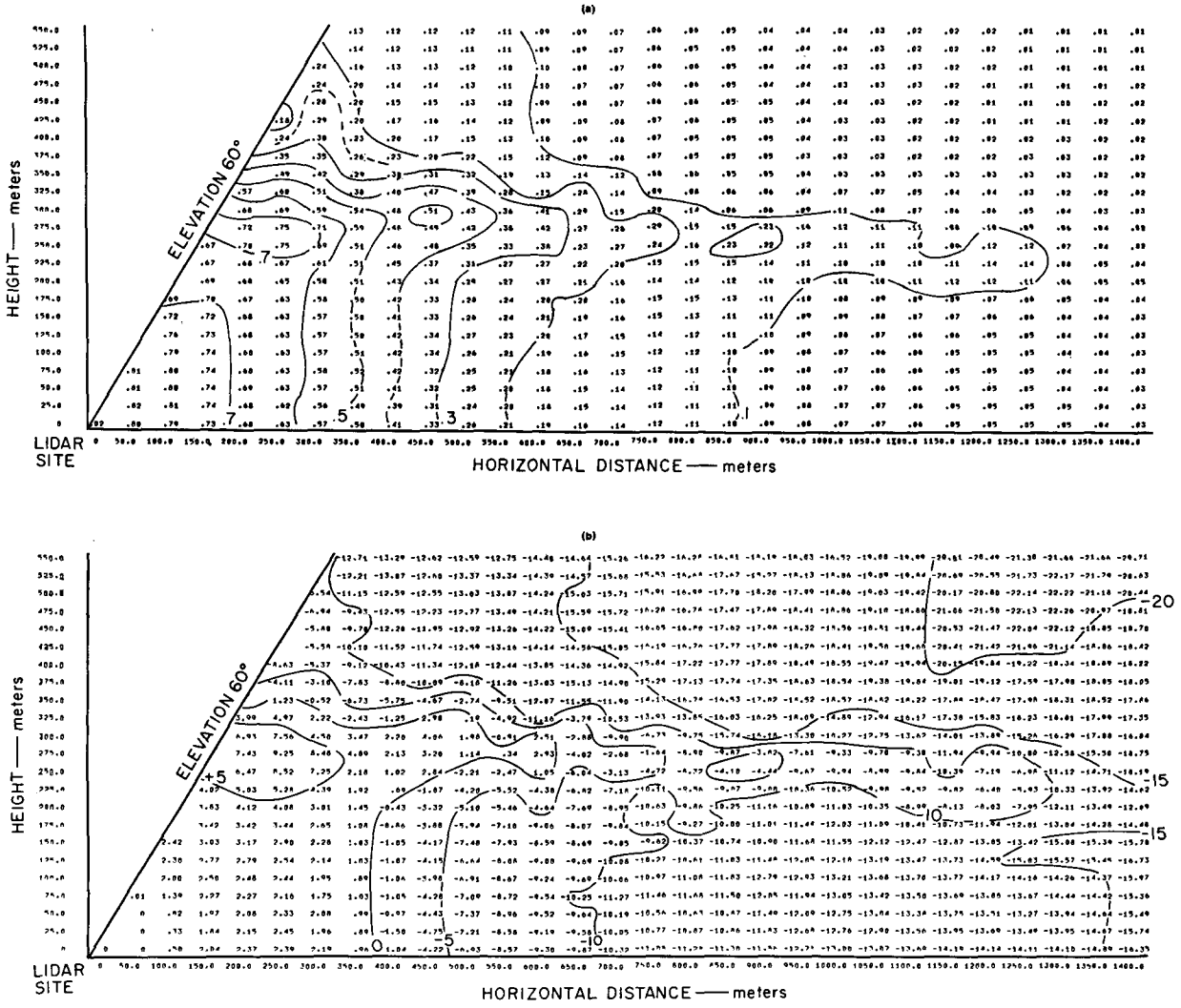

FIG. 7. Computer printout for grid-point analysis of oscilloscope deflection in relative voltage (a), and S function in relative dB (b), in the vertical plane of lidar observation (Hamilton AFB, 8 January 1968, 2222–2231 PST).

signature data points was 25 m. The oscilloscope-deflection analysis of Fig. 7a provides a field that is representative of atmospheric scattering activity. The layer of maximum scattering activity at a height of 275 m is related to the level of low clouds shown in the hand analysis of the same date in Fig. 3c.

It is possible to transform the voltage field of Fig. 7a into a parameter field more representative of atmospheric conditions and perhaps, in the case of ideal data, into a field of extinction coefficients from which the meteorological range or the "visibility" along any given path (such as along an aircraft landing approach path) may be inferred. Further quantitative analysis of the lidar data uses the lidar equation as a starting point, which can be written in the form

$$P_r(R)=P_t\frac{c\tau}{2}\frac{A_r}{R^2}\beta_{180}(R)T_c(R)\exp\left[-2\int_0^R\sigma(l)dl\right], \quad (1)$$

where P_r is the power collected (at a given instant) by the primary receiver optics from atmospheric backscatter of laser energy, R range, P_t power transmitted into the atmosphere, c the velocity of light, τ the pulse duration, A_r the effective receiver area, $\beta_{180}(R)$ the volume backscatter coefficient, $T_c(R)$ the beam convergence factor, and $\sigma(R)$ the volume extinction coefficient.

The above formulation assumes a constant energy density across the beam, randomly distributed scatterers within the effective scattering volume, and Bouquer's law of attenuation. When the beam convergence factor T_c is excluded, Eq. (1) is valid only at ranges beyond the point where the diverging transmitted beam of the non-coaxial lidar system is fully encompassed by the diverging receiver field of view. By including T_c, Eq. (1) can describe the behavior of the lidar return signal at close-in range. T_c varies between 0 (before beam interception) and 1 (at full beam convergence) and is a function of the specific lidar system used. From (1) a convenient range-corrected quantity, in dB (decibel) notation, can be defined as

$$S(R)\equiv 10\log\left(\frac{P(R)R^2}{P(R_0)R_0^2}\right)$$

$$=10\log\left(\frac{\beta_{180}(R)T_a^2(R)T_c(R)}{\beta_{180}(R_0)T_a^2(R_0)T_c(R_0)}\right), \quad (2)$$

where R_0 is a reference range on each lidar trace and

$$T_a(R)=\exp\left[-\int_0^R\sigma(l)dl\right]$$

is the one-way atmospheric transmission over the range R. Again using the lidar data observed during the evening of 8 January, a grid-point analysis of $S(R)$ was obtained from (2) in the following manner. From a relative calibration of the nonlinear response of the Mark V ruby lidar receiver (including photomultiplier, logarithmic amplifier and oscilloscope), estimated to be valid for the conditions of the Hamilton AFB experiment, a polynomial operator was defined by means of which the computer transforms the output-voltage field of Fig. 7a into a field of relative light $[P_r(R)]$ incident on the primary receiver optics. Using the first data point on each of the 18 lidar observations as the reference range R_0, Fig. 7b shows the computer output of the S function field thus obtained. Large increases and decreases with height correspond to cloud layers. A comparison with the qualitative analysis of the same data shown in Fig. 3c clearly indicates the potential practicability of this computer-produced parameter field for cloud-ceiling determination.

The derivative of $S(R)$ over the range of full beam convergence ($T_c=1$) may be expressed as

$$\frac{dS}{dR}=4.34\frac{1}{\beta}\frac{d\beta}{dR}-8.7\sigma, \quad (3)$$

where the subscript 180 on β and the range-dependence notation (R) have been omitted. A closed-form solution for the optical parameters β and σ requires additional information on the scattering properties of the atmosphere or on a backscatter-extinction relation. When the backscatter coefficient β is independent of range, as is the case in a homogeneous scattering medium, the extinction coefficient between deflection points of $S(R)$ is given by

$$\bar{\sigma}=-\frac{1}{8.7}\frac{\Delta S}{\Delta R}. \quad (4)$$

Fig. 8a presents a computer output of the grid-point analysis of $\bar{\sigma}$ over the complete field of Fig. 7b. Negative values (shaded) and large positive values (unshaded) represent areas where the received lidar signal sharply increases and decreases, respectively. Beyond the range of full beam convergence (100–120 m), these areas correspond to areas of non-constant backscatter and allow inferences as to the levels of low-cloud layers analyzed in Fig. 3c. Thus, the presence of dense stratus clouds is clearly indicated in this computer analysis of the signature slope, even though the initial assumption of a constant β is obviously unreal. The presence of horizontally extensive higher clouds is suggested by the areas of negative values (signal increase) at 500 m. The hand analysis of Fig. 3c shows these clouds only in the high elevation lidar data. Thus, the computer is capable of analyzing small changes in signature slope that escape the eye.

A solution to (3) for the optical parameters β and σ is possible when the existing relation between these

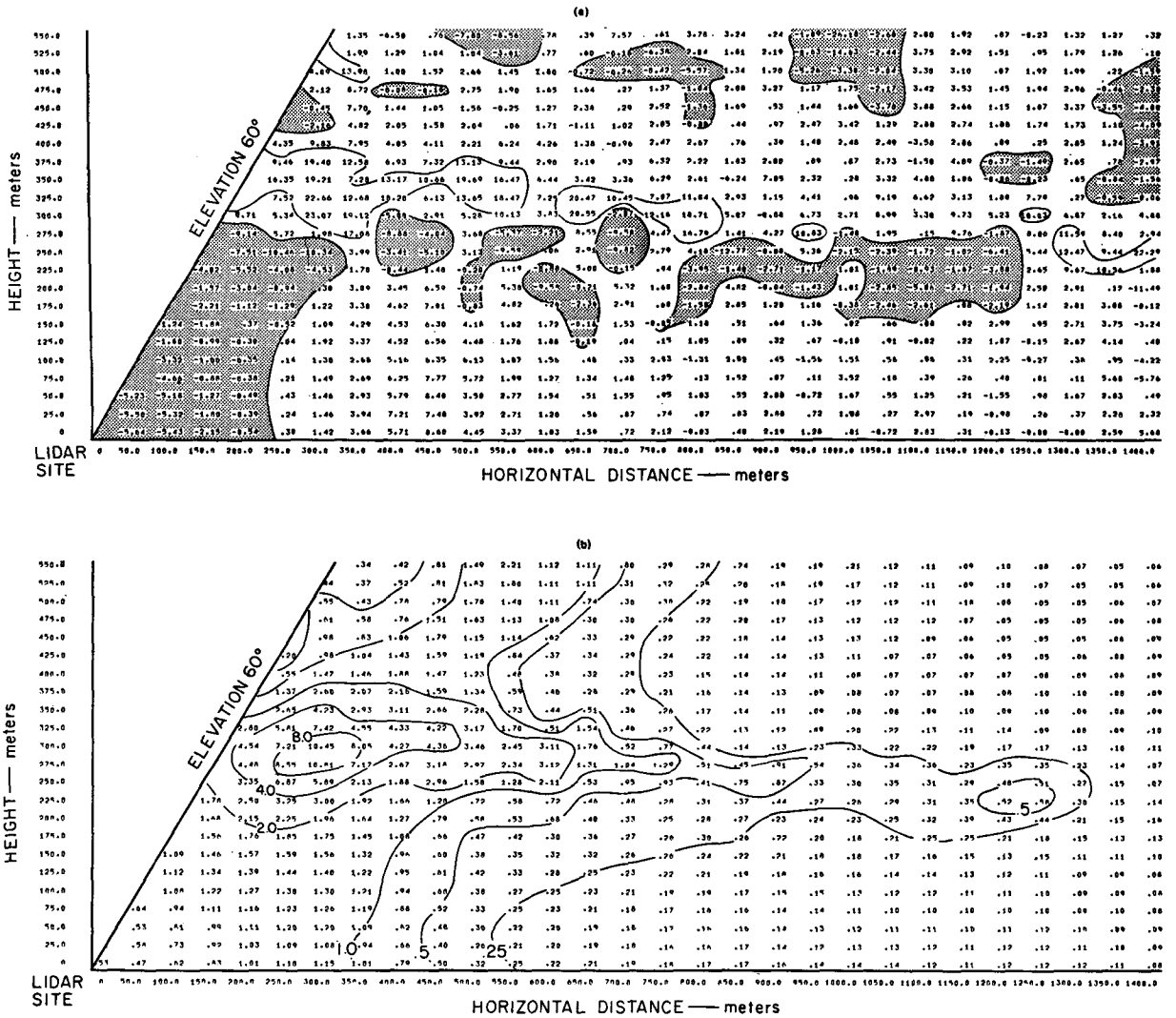

FIG. 8. Computer printout for grid-point analysis of $\bar{\sigma}$ [km^{-1}] assuming constant β (a), and σ [km^{-1}] assuming $d(\ln\beta)/d(\ln\sigma)=k_2$ (b) (Hamilton AFB, 8 January 1968, 2222–2231 PST).

quantities is known. Fenn (1966), using the data of Barteneva (1960), and Curcio and Knestrick (1958) have shown that a relation such as

$$\frac{d(\ln\beta)}{d(\ln\sigma)}=\text{constant}=k_2 \tag{5}$$

is valid within 20–30% for extinction coefficients between 0.01 and 1.0 km^{-1} when employing a broad spectral source. Assuming such a relation to be valid for the conditions of this experiment, substitution of (5) into (3) yields a first-order nonlinear differential equation

$$\frac{d\sigma}{dR}-C_1\frac{dS}{dR}\sigma-C_2\sigma^2=0,$$

where $C_1=1/4.34\,k_2$ and $C_2=2/k_2$. The transform $\eta=1/\sigma$ reduces this differential equation to the linear form

$$\frac{d\eta}{dR}+C_1\frac{dS}{dR}\eta+C_2=0, \tag{6}$$

for which the solution may be written as

$$\sigma(R)=\exp[C_1S(R)]\left\{C_I-C_2\int_R\exp[C_1S(l)]dl\right\}^{-1}, \tag{7}$$

where C_I is the constant of integration.

Solution for multiple traces requires a boundary value for each trace or correction and/or assumptions on lidar variable parameters between traces. The method used

in the analysis of the present lidar data was to obtain a boundary value of extinction coefficient from the slope technique for part of a signature for which the backscatter was thought to be constant with range. The solution was then taken along this trace in the direction of the lidar. Boundary values of σ at the initial data point (range R_0) for each additional trace were derived assuming unity transmission of the lidar energy to these data points and the initial value of σ from the trace containing the boundary point. Extinction coefficients were then evaluated for each data point in the field. A value of 1.4 was assigned to the constant k_2. Such a value probably underestimates the attenuation of the lidar energy and thus decreases the probability of a singularity

$$\left\{C_I = C_2 \int_R \exp[C_1 s(l)]dl\right\}$$

in Eq. (7). The validity of the solution field is determined by rederiving the S functions from the right-hand term of (2) from evaluated quantities.

Fig. 8b presents the grid-point analyses of the σ field obtained. As in the previous computer analyses, the level of the low clouds is clearly shown by large values and large vertical gradients of σ. By comparison with Fig. 7b, it is clear that some of the attenuation effect has been removed from the data field. However, the nonhorizontal isopleths indicate that additional attenuation should be accounted for by employing a smaller value of k_2 or a larger value of the boundary extinction coefficient. Further experimentation along these lines was not considered justified because of the limited quantity and quality of the data. The real merit of a derived σ field is that transmission along any line segment defined by two points in the field may be evaluated and thus slant-range visibilities inferred.

b. *Discussion*

Figs. 7 and 8 show the operational feasibility of describing the spatial distribution of cloud ceiling and low-cloud structure with a lidar-electronic computer combination. The results shown are not considered optimum since they depend on several assumptions that may be relaxed or altered through further investigations. The primary uncertainty is the validity of the assumed β-σ relation and the assumed single scattering involved in the solution of (3). It is suggested in future experiments of the type described in this report that the neodymium laser be used because of its broader spectral energy (100 Å) in comparison to that of the ruby laser. The broad spectral characteristic gives more validity to assuming a β-σ relation (Twomey and Howell, 1965). Also necessary is some further research in the numerical application of (7). For example, various boundary values can be evaluated by using a completely calibrated lidar or by using an extinction coefficient derived from the return of the lidar energy from a ground-based target of known reflectivity.

5. Conclusions

A limited experiment in the use of lidar for the determination of cloud ceiling has been described. The conditions during the experiment, although ideal from a meteorological point of view, were by no means optimum in terms of equipment or experimental procedures. For example, the use of the neodymium (10,600 Å) version of the Mark V lidar, capable of firing every 4–5 sec would have been preferable; also more complete calibration and reference-measurement procedures are desirable. However, the results demonstrate a real potential of lidar for use in operational determinations of aircraft landing conditions when low clouds are present and the cloud base is ragged and diffuse. Currently, such conditions can not be adequately described because the standard observational techniques are limited to measuring cloud base height (or ceiling) and horizontal visibility at a single point. An optimum technique must be able to determine conditions *along* the landing approach path and must provide information on the slant visibility to the ground from *any* point along that path. Because of its ability to remotely monitor the cloud ceiling at various locations distant from the point of observations, the lidar does approach the optimum technique of describing conditions along the glide path. The possibility of processing lidar observations to obtain quantitative data on the extinction coefficient, i.e., the optical parameter significant to "visibility" determinations, needs to be explored further. However, the objective determination of a cross section showing a field of values that are related to atmospheric scattering activity and that portray conditions of low-cloud ceiling and reduced horizontal visibility is considered to be a major advance in this problem area.

It is obvious that much remains to be done. For simple graphical description of the cloud base, further work is necessary on the physical interpretation of inflections on the lidar signature, and also on the technique of processing and displaying data. The conversion of lidar observations to digital form for computer processing, and the computational solutions themselves also need further development.

Finally, in any routine operational application of lidar due consideration must be given to all aspects of eye safety.

Acknowledgments. The cooperation and hospitality received during the field observations from Col. Harry W. Shoup, USAF, Commander 78th Fighter Wing, Hamilton AFB and from Col. Leroy C. Iverson, USAF, and Lt. Col. Milton Plattner, USAF, Commander and Deputy Commander, respectively, of 35th Weather

Squadron are gratefully acknowledged. Special credit is due to Capt. Robert H. Hedenberg, USAF, Commander, Det. 9, 35th Weather Squadron, for his assistance throughout the project.

REFERENCES

Barteneva, O. D., 1960: Scattering functions of light in the atmospheric boundary layer. *Bull. Acad. Sci. USSR, Geophys. Ser.*, No. 12, 1852.

Curcio, J. A., and G. L. Knestrick, 1958: Correlation of atmospheric transmission with backscattering. *J. Opt. Soc. Amer.*, **48**, 686–689.

Endlich, R. M., and R. L. Mancuso, 1968: Objective analysis of environmental conditions associated with severe thunderstorms and tornadoes. *Mon. Wea. Rev.*, **96**, 342–349.

Fenn, R. W., 1966: Correlation between atmospheric backscattering and meteorological visual range. *Appl. Opt.*, **5**, 293–295.

Twomey, S., and H. B. Howell, 1965: The relative merit of white and monochromatic light for the determination of visibility by backscattering measurements. *Appl. Opt.*, **4**, 501–506.